1521-009X/51/3/276–284$35.00
DRUG METABOLISM AND DISPOSITION

dx.doi.org/10.1124/dmd.122.001132
Drug Metab Dispos 51:276–284, March 2023

Quantitative Cytochrome P450 3A4 Induction Risk Assessment Using Human Hepatocytes Complemented with Pregnane X Receptor-Activating Profiles[S]

Aynur Ekiciler,[1] Wen Li Kelly Chen,[1] Yan Bo, Alessandra Pugliano, Massimiliano Donzelli, Neil Parrott, and Kenichi Umehara

Roche Pharmaceutical Research and Early Development, Roche Innovation Center Basel, Basel, Switzerland (A.E., A.P., M.D., N.P., K.U.) and Roche Pharmaceutical Research and Early Development, China Innovation Center of Roche, Shanghai, China (W.L.K.C., Y.B.)

Received September 23, 2022; accepted November 23, 2022

ABSTRACT

Reliable in vitro to in vivo translation of cytochrome P450 (CYP) 3A4 induction potential is essential to support risk mitigation for compounds during pharmaceutical discovery and development. In this study, a linear correlation of CYP3A4 mRNA induction potential in human hepatocytes with the respective pregnane-X receptor (PXR) activation in a reporter gene assay using DPX2 cells was successfully demonstrated for 13 clinically used drugs. Based on this correlation, using rifampicin as a positive control, the magnitude of CYP3A4 mRNA induction for 71 internal compounds at several concentrations up to 10 μM ($n = 90$) was predicted within 2-fold error for 64% of cases with only a few false positives (19%). Furthermore, the in vivo area under the curve reduction of probe CYP substrates was reasonably predicted for eight marketed drugs (carbamazepine, dexamethasone, enzalutamide, nevirapine, phenobarbital, phenytoin, rifampicin, and rufinamide) using the static net effect model using both the PXR activation and CYP3A4 mRNA induction data. The liver exit concentrations were used for the model in place of the inlet concentrations to avoid false positive predictions and the concentration achieving twofold induction (F2) was used to compensate for the lack of full induction kinetics due to cytotoxicity and solubility limitations in vitro. These findings can complement the currently available induction risk mitigation strategy and potentially influence the drug interaction modeling work conducted at clinical stages.

SIGNIFICANCE STATEMENT

The established correlation of CYP3A4 mRNA in human hepatocytes to PXR activation provides a clear cut-off to identify a compound showing an in vitro induction risk, complementing current regulatory guidance. Also, the demonstrated in vitro–in vivo translation of induction data strongly supports a clinical development program although limitations remain for drug candidates showing complex disposition pathways, such as involvement of auto-inhibition/induction, active transport and high protein binding.

Introduction

Enzyme induction, defined as the increase in the biosynthesis of catalytically active enzyme following exposure to a chemical agent, is an important mechanism of pharmaceutical drug–drug interaction (DDI). The associated increase in the metabolism and clearance of a drug [either the inducing molecule itself (auto-induction) or a co-medication], can lead to reduced pharmacological activity or even toxicity due to increased metabolite levels. These potential effects on efficacy and safety mean that the induction of cytochrome P450 (CYP) enzymes is of high clinical importance (Hakkola et al., 2020).

CYP induction occurs mainly via aryl hydrocarbon receptor for CYP1A, constitutive androstane receptor (CAR) for CYP2B6, and pregnane X receptor (PXR) for CYP3A. Many other enzymes [(e.g., CYP2C8, CYP2C9, CYP2C19, uridine 5′-diphospho-glucuronosyltransferase] and transporters [e.g., P-glycoprotein] are also induced via the PXR pathway (Yamazaki et al., 2019, Lu and Di, 2020). Since CYP3A4 metabolizes more than 50% of clinically used drugs, PXR activation is of primary clinical relevance (Lehmann et al., 1998, Einolf et al., 2014). CYP3A4 induction involves the steps of transcription and translation and is a dynamic complex process (Yamashita et al., 2013).

This work was supported by F. Hoffmann-La Roche.
A.E., W.L.K.C., Y.B., A.P., M.D., N.P., and K.U. are employees of F. Hoffmann-La Roche.
[1]A.E. and W.L.K.C. share the first authorship.
dx.doi.org/10.1124/dmd.122.001132.
[S] This article has supplemental material available at dmd.aspetjournals.org.

ABBREVIATIONS: AUC, area under the curve; AUCR, area under the curve ratio; CAR, constitutive androstane receptor; Cave, average concentration at steady state; Cmax, maximum steady state concentration; Cave,u, unbound average concentration at steady state; Cmax,u, unbound maximum steady state concentration; Ct, cycle time; ΔCt, the change in Ct for gene of interest relative to housekeeping gene; ΔΔCt, the change in ΔCt for test compound relative to vehicle control (i.e., fold induction); CYP, cytochrome P450; DDI(s), drug–drug interaction(s); Emax, maximum fold increase (or induction) minus baseline of 1-fold; F2, the concentration achieving 2-fold induction; Fa, fraction absorbed after oral administration; Fg, fraction available escaped from intestinal metabolism after oral administration; fu, fraction unbound in plasma; GAPDH, glyceraldehyde 3 phosphate dehydrogenase; ka, absorption rate constant; PBPK, physiologically-based pharmacokinetic; PCR, polymerase chain reaction; P-gp, P-glycoprotein; PXR, pregnane-X receptor; Qent, enterocyte blood flow rate; RT-PCR, real-time reverse-transcription polymerase chain reaction.

Nonetheless, mechanistic static model approaches based on the ratio of in vivo peak plasma concentration to the half-maximal effective concentrations (EC50) for CYP3A4 mRNA induction in human primary hepatocytes or liver-derived HepaRG cells have shown reasonable prediction of clinical induction potential (Kanebratt and Andersson, 2008, Einolf et al., 2014). Furthermore, 20 clinical DDI study results where greater than 20% decreases in the exposure of CYP3A4 substrates in the presence of moderate and strong inducers could be predicted with physiologically-based pharmacokinetic (PBPK) modeling (Bolleddula et al., 2021). These approaches may also predict the induction of intestinal CYP3A4 by taking into account intestinal enzyme abundance. Guidelines for investigation of induction DDI risk with both static and dynamic modeling have been provided by regulators (Huang et al., 2013, Luzon et al., 2017, Sato et al., 2017) and international harmonization efforts are in progress (ICH M12). Recently, the International Consortium for Innovation and Quality PBPK induction Working Group proposed initial roadmaps for PBPK application for induction DDI risk assessment and discussed future trends based on a survey across participating pharmaceutical industries (Hariparsad et al., 2022).

While the pharmaceutical industry follows these guidance documents for induction risk assessment, several scientific gaps remain, and different stages of drug discovery and development are still subject to uncertainties and challenges. PXR binding and reporter gene assays have been deployed as high-throughput screening assays in drug discovery (Zhu et al., 2004) and attempts to correlate CYP3A4 induction in human hepatocytes to PXR fold activation in a reporter gene assay have been made for 14 reference drugs (Luo et al., 2002). However, there have been limited reports on use of these data for prediction of the magnitude of in vivo CYP3A4 induction for marketed drugs or pharmaceutical development compounds. Another important consideration for mechanistic model-based induction predictions is that the DDI risk assessment can be highly impacted by the reliability of in vitro input parameters. For instance, cytotoxicity or solubility limitations at higher concentrations mean that reliable estimation of in vitro induction parameters such as EC50 can be challenging. For this reason, the concentration achieving twofold induction (F2) was recently proposed as an alternative to EC50 (Kenny et al., 2018) and has been used in this study.

In this work, we aimed to establish a correlation of PXR activation in a reporter gene assay to CYP3A4 mRNA induction in human hepatocytes for 13 clinically used CYP3A4 inducers taken from the United States Food and Drug Administration DDI guidance document. This has been followed by the application of the obtained in vitro–in vitro correlation to make predictions for 71 internal drug discovery compounds. Finally, we wished to compare the translatability to in vivo of the data from the PXR reporter gene assay with that of the hepatocyte mRNA assay and to assess their potential for induction DDI risk mitigation. This evaluation used a set of clinical DDI data collected from the literature for 10 marketed drugs which are known enzyme inducers. A mechanistic PBPK modeling approach would be ideal to capture the dynamic changes involved in vivo including enzyme transcription/translation dynamics and potential negative feedback on PXR. However, such a modeling approach remains challenging (Yamashita et al., 2013). Therefore, our predictions of the effect of CYP3A4 induction on the exposure of reference CYP3A4 substrates was performed within a mechanistic static model using the F2 parameter derived from in vitro.

Materials and Methods

Chemicals. Carbamazepine, dexamethasone, nevirapine, nifedipine, phenobarbital, phenytoin, pleconaril, rifampicin, ritonavir, rufinamide, sulfinpyrazone, and tamoxifen were purchased from Sigma-Aldrich (St. Louis, MO). Efavirenz and mitotane were obtained from Abcam (Cambridge, United Kingdom). Enzalutamide, etravirine, and flumazenil were purchased from TargetMol (Wellesley Hills, MA), Cayman Chemical (Ann Arbor, MI), and National Institute for Food and Drug Control (Beijing, China), respectively. Bosentan and drug candidates ($n = 71$) from early drug discovery phases were synthesized at F. Hoffmann-La Roche Ltd. (Basel, Switzerland). DMSO (Sigma-Aldrich) was used to prepare stock solutions of the test drugs, resulting in the designated DMSO concentrations (%, v/v) in the final incubation samples.

PXR Reporter Gene Assay. DPX2 cells, a HepG2-derived cell line stably integrated with a PXR expression vector plus a luciferase reporter (Fahmi et al., 2012), were plated in 96-well plates in a Puracyp culture medium (Carlsbad, CA) supplemented with 10% (v/v) fetal bovine serum at a cell density of 4.5×10^5 cells/ml. After approximately 24 hours, the plating medium was replaced by medium containing test articles at concentrations of 0.1–10 μM and including the positive control activator rifampicin at 20 μM in a vehicle solvent control (0.1% v/v DMSO). The cultures were maintained for 48 hours. Flumazenil at 0.1–10 μM was also tested as a negative control. After the treatment, the dosing medium was aspirated from each well and, washed twice with PBS. The PXR reporter activity (luminescence) of the treated cells in the individual wells was determined with the ONE-Glo Luciferase assay kit and cell viability was determined by CellTiter-Fluor Cell Viability Assay kit according to the supplier's specifications (http://www.puracyp.com/). All incubations were performed in triplicate.

Human Hepatocyte Culture and Incubation with the Test Article. Human hepatocytes from individual human liver donors were acquired from Corning Life Sciences (Woburn, MA) [Batch No. 399 (female, 27 years old)], LONZA (Walkersville, MD) [HUM182641 (male, 4 years old), HUM181441 (male, 53 years old) and HUM180871 (female, 37 years old)] and KaLy-Cell (Plobsheim, France) [S1554T (male, 68 years old)]. The following assays were performed according to (Zhang et al., 2014) with some modifications.

The inducible cryopreserved hepatocytes were thawed rapidly and purified followed by plating on 24- or 96-well collagen I-coated plates at 0.6 or 0.06×10^6 cells/well, respectively, using high viability cryo-hepatocyte recovery kits (In Vitro ADMET Laboratories, LLC; Columbia, MD). After approximately 4 hours, the plating medium was replaced with hepatocyte culture medium (Corning Life Sciences), and the cultures were maintained overnight. Hepatocyte cultures were treated for 2 days with test articles at 0.1, 1, 3, and 10 μM. The medium was replaced daily with fresh hepatocyte culture medium containing the test article or controls. After a total of 48 hours of treatment of the induction assessment, medium was aspirated from the wells, and the cells were washed twice with pre-warmed Hanks' Balanced Salt Solution containing 10 mM HEPES and then stored at -80°C before real-time reverse-transcription polymerase chain reaction (RT-PCR) assays. The positive control inducers of CYP2B6 were 1000 or 2000 μM phenobarbital and for CYP3A4 1 or 10 μM rifampicin in a vehicle solvent control (0.1% v/v DMSO). Flumazenil at 0.1–10 μM was also tested as a negative control. All incubations were performed in triplicate.

After hepatocytes were exposed to the test articles and the positive control cytotoxic agent tamoxifen (50 μM) or doxorubicin (100 μM), the hepatocyte viability in culture was also tested using the 3-[4, 5-dimethyl-2-thiazolyl]-2, 5-diphenyl-2H-tetrazolium bromide assay (Corning Life Sciences) or the lactate dehydrogenase assay (F. Hoffmann-La Roche Ltd) according to the corresponding manufacturer's instruction. The hepatocytes were also visually inspected for cellular morphology during the treatment period. All incubations were performed in triplicate.

Total RNA Isolation and Reverse Transcription Polymerase Chain Reaction (RT-PCR) Assays. The 48-hour treated plates were thawed at room temperature and RNA isolation was performed manually using the RNeasy kit (Qiagen, Germany) or the Taqman Fast Cells kit (Thermo Fisher; Waltham, MA) according to the manufacturer's instructions. The mRNA expression for each CYP was determined by Taqman Real Time RT-PCR methods. An RT assay was performed using a GeneAmp PCR system 9700 (Thermo Fisher) followed by a PCR assay conducted with a ViiA7 PCR system (Thermo Fisher); otherwise a one-step RT-PCR assay was performed with LightCycler 480 (F. Hoffmann-La Roche Ltd) or CFX96 Touch Real-Time PCR Detection System (Bio-Rad; Hercules, CA): RT reaction for 60 minutes at 37°C followed by inactivation for 5 minutes at 95°C; and PCR reaction (40 cycles) for 1 second at 95°C followed by 20 seconds at 60°C. The following probes (Thermo Fisher) were used in the PCR assay: β-actin (Hs99999903_m1) or glyceraldehyde 3-phosphate dehydrogenase (Hs02786624_g1) for the housekeeping gene,

CYP2B6 (Hs03044634_m1 or Hs04183483_g1) and CYP3A4 (Hs00430021_m1 or Hs00604506_m1).

Data Calculation in the Human PXR Activation and Hepatocyte Induction Assays. Regarding the reporter gene assay, the normalized luciferase activity was determined by a ratio of $(RLU/RFU)_{test\ substance}$ per $(RLU/RFU)_{vehicle}$, where the RLU and RFU represents the mean luminescence unit and the mean fluorescence unit, for each test compound at each dosage and for vehicle, respectively.

The fold induction for CYP2B6 and/or CYP3A4 mRNA in human cryopreserved hepatocytes was determined using the calculation of $2^{-\Delta\Delta Ct}$ (Livak and Schmittgen, 2001) where ΔΔCt represents the change in ΔCt for test compound relative to vehicle control (i.e., fold induction). The ΔCt value is determined by the change in the fractional PCR cycle numbers (Ct) for a target gene (CYP2B6 and/or CYP3A4) relative to a corresponding endogenous control gene (β-actin or glyceraldehyde 3 phosphate dehydrogenase).

Percentage (%) of positive control response for both PXR activation and CYP3A4 mRNA induction were calculated as follows: (mean of observed fold increase - 1)/(mean of observed maximal fold increase by rifampicin -1). Rifampicin at 20 μM and 10 μM were considered as control to provide the 20–40 fold enhancement as a maximal-fold readout in the PXR activation and hepatocyte induction assays, respectively. This allowed relatively good resolution in % of control data assessment. As an exception, the 20–40 fold-induction of CYP3A4 mRNA at 1 μM rifampicin was used as control in two liver donors (HUM182641 and HUM180871), which showed a fold-induction of ~100 at 10 μM throughout the study. This was aligned with the criteria previously proposed that the magnitude of maximal rifampicin response in the donor should be ≥ 10-fold irrespective of positive or negative for CYP3A4 mRNA induction (Kenny et al., 2018).

The fold value and % of the positive control response in the reporter gene assay were compared with the corresponding readout in the human hepatocyte induction assay for 13 marketed drugs including the index inducers for CYP3A4 defined in the DDI guidance document. After that, a linear regression correlation established from the training data set was applied to predict CYP3A4 mRNA induction potential for 71 internal drug candidates synthesized at F. Hoffmann-La Roche Ltd.

Curve Fitting. To estimate the drug concentration that causes a 2-fold increase in PXR activation or CYP induction value in the reporter gene and hepatocyte assays, the concentration-dependent induction response data were fitted to eq. 1:

$$F2 = \frac{2}{(Top\ -\ 1)^{(1/2)\times EC50,\,app}} \tag{1}$$

where Top and EC50,app are the apparent maximal response and the concentration achieving 50% of the Top value, respectively (Zhang et al., 2014; Kenny et al., 2018). The curve fitting was performed using Phoenix 64 (Certara Inc., Princeton, NJ).

Correlation Approaches. The net effect eq. 2 was used to predict the magnitude of the DDIs expressed as the ratio of area under the exposure-time curve in the presence and absence of CYP3A4 induction (AUCR) (Fahmi et al., 2009). The impact of competitive inhibition and inactivation on CYP3A4 in the intestine and liver was omitted from the mathematical model.

$$AUCR = \frac{1}{Cg \times (1 - Fg) + Fg} \times \frac{1}{Ch \times fm + (1 - fm)} \tag{2}$$

In eq. 2, Fg and fm are the fraction escaping intestinal metabolism and the fraction metabolized by CYP3A4, respectively. Cg and Ch are the terms for induction in the intestine and the liver, respectively. These terms include the ratios of the in vivo concentrations where the DDI occurs ([I]h and [I]g for liver and gut, respectively) to the respective F2 values obtained from the PXR activation or hepatocyte induction study results.

$$Ch = 1 + \frac{[I]h}{F2} \tag{3}$$

$$Cg = 1 + \frac{[I]g}{F2} \tag{4}$$

[I]g was estimated according to eq. 5 (Yang et al., 2007).

$$[I]g = \frac{ka \times Fa \times Dose}{Qent} \tag{5}$$

where ka, Fa and Qent are oral absorption rate constant, fraction absorbed of oral dosing, and enterocyte blood flow rate (18 L/h), respectively. For liver, several options were considered: [I]h = average concentration at steady state (Cave, method 1), unbound Cave (Cave,u; method 2), maximum steady state concentration (Cmax, method 3), and unbound Cmax (Cmax,u; method 4). The current static model did not consider the interplay between enzyme induction and degradation rate of CYP3A4. The differences of the currently deployed and original net effect models are briefly summarized in Table 1.

Finally, 31 in vivo DDI study results for 10 marketed inducer drugs (carbamazepine, bosentan, dexamethasone, enzalutamide, nevirapine, phenobarbital, phenytoin, pleconaril, rifampicin, and rufinamide) found by searching the University of Washington Drug Interaction Database (https://didb.druginteractionsolutions.org/) were compared with the magnitude of the CYP3A4 induction potential predicted based on the modified net effect model above. The observed DDI study data used as reference are summarized in Table 2. The in vivo sensitive CYP3A4 substrates used in the reference clinical DDI studies were cyclosporine, itraconazole, panobinostat, triazolam, verapamil, simvastatin, and midazolam. A head-to-head comparison with the static induction DDI risk prediction results was made in this study. The respective Fg and fm values were as follows: 0.48 (Davies et al., 2020) and 0.99 (SimCYP V21 prediction) for cyclosporine; 0.94 and 0.98 (SimCYP V21 prediction) for itraconazole; 0.68 and 0.40 (Einolf et al., 2017) for panobinostat; 0.36 (Masica et al., 2004) and 0.93 (Klammers et al., 2022) for triazolam; 0.60 (Davies et al., 2020) and 0.65 (SimCYP V17 model verification document) for verapamil; 0.29 (Davies et al., 2020) and 1 (Klammers et al., 2022) for simvastatin; and 0.57 (Vieira et al., 2014) and 0.95 (Njuguna et al., 2016) for midazolam.

TABLE 1

A summary of the net effect model equation used in this study for the induction DDI risk prediction in comparison with the original model

Net effect model:

$AUCR = \frac{1}{Ag \times Bg \times Cg \times (1 - Fg) + Fg} \times \frac{1}{Ah \times Bh \times Ch \times fm + (1 - fm)}$

A: effects of reversible inhibition (=1 in this study)
B: effects of time-dependent inhibition (=1 in this study)
C: effects of induction
Fg: fraction available after intestinal metabolism (0.57 for midazolam) (Vieira et al., 2014)
fm: fraction metabolized by a CYP enzyme of the probe substrate (0.95 for midazolam) (Njuguna et al., 2016)
h and g denote liver and gut, respectively

		Method 1	Method 2	Method 3	Method 4
New model in this study: F2	$Ch = 1 + [I]h/F2$ $Cg = 1 + [I]g/F2$	$[I]h = Cave$	$[I]h = Cave,u$ $[I]g = ka \times Fa \times Dose/Qent$	$[I]h = Cmax$	$[I]h = Cmax,u$
Original model: EC50/Emax		$Ch = 1 + \frac{d \times Emax \times [Ih]}{[Ih] + EC50}$, where $[I]h = fu \times (Cmax + ka \times Fa \times Dose/Qent/Rb)$			
		$Cg = 1 + \frac{d \times Emax \times [Ig]}{[Ig] + EC50}$, where $[I]g = ka \times Fa \times Dose/Qent$			

d, a scaling factor assumed to be 1 unless an internal induction calibrator is available; Rb, blood-to-plasma ratio. Qh: 97 L/h, Qent: 18 L/h (Yang et al., 2007).

Results

Qualification of Hepatocyte Batches for Inducibility of CYP Enzymes and DPX2 Cells for PXR Activation. As CYP3A4 induction may be co-regulated by PXR and CAR activation (Einolf et al., 2014), the enzyme inducibility of hepatocyte batches used in this study (e.g., lot. 399) was confirmed by measurement of the fold increases in mRNA for CY3A4 (PXR) and CYP2B6 (CAR) after exposure to concentration-dependent (1, 3, and 10 μM), strong (carbamazepine, phenytoin), moderate (efavirenz), and weak (dexamethasone) CYP3A4 inducers (Supplemental Figure 1). Phenobarbital at 1000 or 2000 μM, and rifampicin at 10 μM were used as the positive control inducers for CYP2B6 and CYP3A4, respectively. Of note, one batch (S15554T) excluded from the current study showed a concentration-dependent increase in CYP3A4 mRNA, but a similar increase could not be demonstrated in CYP2B6 mRNA (Supplemental Figure 1). No cytotoxic signals were observed among all the test substances used in this study except for efavirenz at 10 μM.

Despite the inter-individual variability, all human hepatocyte batches selected for this study (399, HUM181441, HUM180871 and/or HUM182641) showed a concentration-dependent CYP3A4 mRNA induction reaching >2-fold up to 10 μM for all test articles apart from pleconaril (Supplemental Table 1). As a negative control, flumazenil showed similar or only slightly higher responses (3.5–4.1% of control) relative to the vehicle control (Supplemental Table 1). Concentration-dependent PXR activation was also observed in DPX2 cells.

PXR Activation Using a Reporter Gene Assay Relative to CYP3A4 mRNA Induction in Cultured Human Hepatocytes. For a set of 13 marketed in vitro and in vivo inducers of CYP3A4 (carbamazepine, dexamethasone, efavirenz, enzalutamide, etravirine, mitotane, nevirapine, nifedipine, phenytoin, pleconaril, ritonavir, rufinamide, sulfinpyrazone), including a negative control (flumazenil) at 0.1, 1, and 10 μM (Fig. 1; Supplemental Table 1). The CYP3A4 mRNA fold-induction and % of the control response were approximately 1.98 and 1.24 times higher than the respective PXR activation data in DPX2 cells showing a good linear correlation with r^2 values of 0.780 and 0.722, respectively.

Since data showing moderate-to-strong PXR activation and CYP3A4 mRNA induction in vitro were limited (Fig. 1), the validity of the correlation and regression analysis results shown in Fig. 1 was further explored by prediction of the CYP3A4 mRNA fold induction using PXR activation data for 71 internal drug candidates at 0.1, 1, and/or 10 μM (Fig. 2). Percentage of the control response was used for this purpose since the readout from the two different in vitro assays was being compared. Nineteen percent of the total data points ($n = 90$) demonstrated >2-fold underestimation of the CYP3A4 mRNA induction potential, 17% showed >2-fold overestimation prediction while 64% were successfully predicted within 2-fold error. The established linear correlation can estimate CYP3A4 mRNA induction using the PXR activation data with a limited number of false negative cases (Fig. 2). Furthermore, when considering the data within different chemical series, the predictive relationship could potentially be modulated based upon a training dataset to improve the predictions for further compounds within the same project. For example, compounds synthesized for project A in Fig. 2 tended to show an overestimation of the CYP3A4 mRNA induction potential.

In Vitro–In Vivo Extrapolation of CYP3A4 Induction Effects. The mean of the % reduction in area under the curve (AUC) observed in clinical DDI study for eight of ten marketed inducer drugs

TABLE 2

Observed clinical induction drug-drug interactions for well-established CYP3A4 substrates

Drug name	Dose (mg)	Route	Frequency	Duration (days)	CYP3A substrate	Dose (mg)[b]	Route	AUC reduction (%)	Mean (SD)
Carbamazepine	300	Oral	b.i.d.	26	Midazolam	2	Oral	79.3	N.A.
Dexamethasone	20	Oral	—	21	Panobinostat	20	Oral (at steady-state)	23.1	N.A.
Enzalutamide	160	Oral	q.d.	85	Midazolam	2 (ss)	Oral	85.9	N.A.
Nevirapine	200	Oral	q.d.	7	Itraconazole	200 (ss)	Oral	62.3	N.A.
Phenobarbital [a]	100	Oral	q.d.	21	Verapamil	80	Oral	76.6	78.0 (N.A.)
	100	Oral	q.d.	21	Verapamil	80 (ss)	Oral	79.4	
Phenytoin	750-1000	Intravenous	q.d.	7	Cyclosporine	75 (ss)	Oral	69.2	N.A.
Rifampicin [1)]	450	Oral	q.d.	5	Midazolam	0.075	Oral	55.9	87.6 (9.88)
	300	Oral	q.d.	7	Midazolam	1	Oral	70.9	
	300	Oral	q.d.	7	Midazolam	1	Oral	79.9	
	450	Oral	q.d.	7	Midazolam	0.015 mg/kg	Oral	83.9	
	600	Oral	q.d.	7	Midazolam	2	Oral	84.2	
	600	Oral	q.d.	11	Midazolam	1	Oral	85.4	
	600	Oral	q.d.	14	Midazolam	2	Oral	86	
	600	Oral	q.d.	9	Midazolam	5.5	Oral	87.6	
	600	Oral	q.d.	28	Midazolam	2	Oral	87.7	
	600	Oral	q.d.	7	Midazolam	4 or 6	Oral	89.7	
	600	Oral	q.d.	15 (average)	Midazolam	2	Oral	90.3	
	600	Oral	q.d.	17	Midazolam	2	Oral	91.2	
	600	Oral	q.d.	14 (average)	Midazolam	2	Oral	91.9	
	300	Oral	b.i.d.	7	Midazolam	8	Oral	94	
	300	Oral	b.i.d.	7	Midazolam	8	Oral	94.3	
	600	Oral	q.d.	5	Midazolam	3	Oral	94.7	
	450	Oral	q.d.	5	Midazolam	7.5	Oral	94.8	
	600	Oral	q.d.	7	Midazolam	1	Oral	95.6	
	600	Oral	q.d.	5	Midazolam	15	Oral	95.9	
	600	Oral	q.d.	5	Midazolam	7.5 or 15	Oral	98.4	
Rufinamide	400	Oral	b.i.d.	11.5	Triazolam	0.25	Oral	36.7	N.A.
Bosentan	125	Oral	b.i.d.	5.5	Simvastatin	40 (ss)	Oral	34.4	N.A.
Pleconaril	400	Oral	t.i.d.	6	Midazolam	0.075 mg/kg	Oral	34.6	N.A.

N.A., not applicable; b.i.d., twice daily; p.o., by mouth; q.d., once daily; ss, steady state.
Data from University of Washington Drug Interaction Database (https://didb.druginteractionsolutions.org/).
[a] DDI study results following the clinically relevant treatment designs were selected.
[b] Dose is in mg unless otherwise noted.

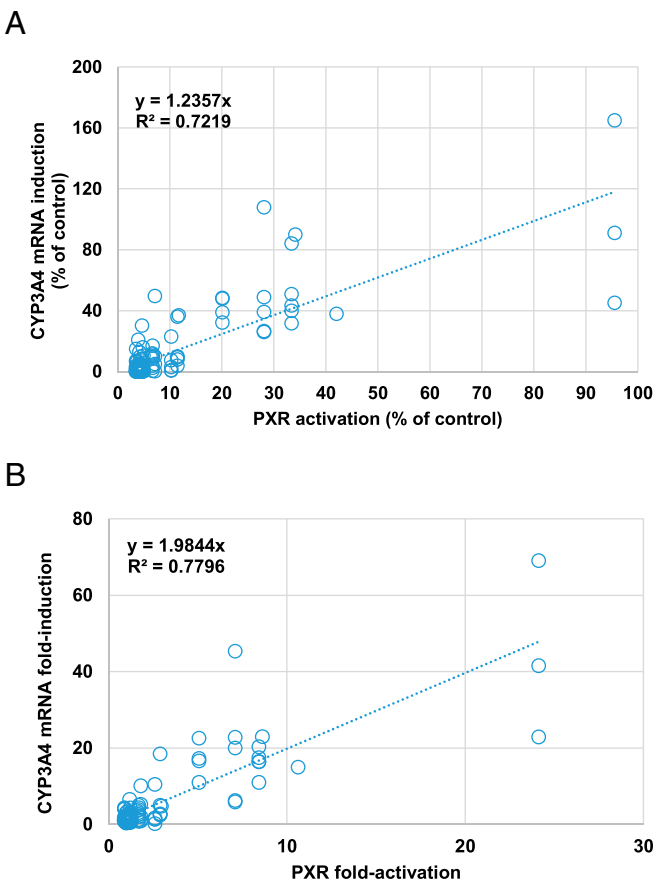

Fig. 1. Correlation between the PXR activation and CYP3A4 mRNA induction. CYP3A4 mRNA induction in human hepatocytes (lots. 399, HUM181441, HUM180871 and HUM182641) after incubation with 14 test substances at 0.1–10 μM (nominal concentrations) for 48 hours (y-axis; mean, n = 3) plotted against PXR activation in DPX2 cells after 48-hour incubation (x-axis; mean, n = 3). Panels (A) and (B) represent the percentage of the control response, and fold-induction/activation, respectively. The raw data used for this analysis are reported in Supplemental Table 1.

(carbamazepine, dexamethasone, enzalutamide, nevirapine, phenobarbital, phenytoin, rifampicin, and rufinamide; Table 2) could be successfully correlated with the CYP3A4 induction potential predicted using the modified net effect model (Table 1 and Table 3; Fig. 3). Correlation did not work for two of ten inducers, namely pleconaril and bosentan (Supplemental Figure 2). The input parameters for the static model calculation are summarized in Supplemental Table 2.

The in vitro–in vivo correlation performance of CYP3A4 induction potential was not affected by the different [I]h values used in the calculation: Cave (method 1), Cave,u (method 2), Cmax (method 3) and Cmax,u (method 4). The induction DDI risk categorization into weak (AUC reduction of the probe CYP3A4 substrate ≦20%), moderate (20%< AUC reduction ≦50%), and strong (50%< AUC reduction ≦80%) was more accurately captured when based on the static prediction results in DPX2 cells [Fig. 3, A, C, E, and G] than when based on the results from cryopreserved hepatocytes where clustering was only achieved into the weak (dexamethasone) and strong induction groups (other 7 drugs) [Fig. 3, B, D, F, and H].

Discussion

Currently, the potential of test articles to induce CYP3A4 is examined primarily by measuring changes in the levels of CYP3A4 mRNA in human cultured hepatocytes. The reporter gene assay with DPX2 cells (Fahmi et al., 2012) has the potential to reduce the need to use inducible human hepatocytes and therefore could be valuable to screen out compounds with CYP3A4 induction potential. However, past reports have noted a relatively poor correlation between PXR activation and CYP3A4 activity, potentially related to the masking of induction by time-dependent inhibition effects (Luo et al., 2002).

In this study, a reasonable correlation of PXR activation in DPX2 cells to CYP3A4 mRNA induction in human hepatocytes for 13 clinically used CYP3A4 inducers was successfully established (Fig. 1, Supplemental Table 1). While ≥20% of the control response has been proposed as a cutoff to identify induction liability, ≥10% of the control response could be proposed as the threshold value for the reporter gene assay since the current study showed that CYP3A4 mRNA induction was approximately 2-fold higher than PXR activation.

Proposals for criteria to identify CYP3A4 induction potential based on the established correlation are summarized in Table 4. Interestingly, relatively weak induction signals of ∼10% of control response were observed in hepatocytes for the two strong in vivo CYP3A4 inducers carbamazepine and phenytoin (Supplemental Table 1). Regarding in vitro data variability, stable PXR activation signals in DPX2 cells were expected with some confidence since the cell lines were stably integrated with a PXR expression vector plus a luciferase receptor (Fahmi et al., 2012). With hepatocytes, considering the highly variable enzyme inducibility among human hepatocyte batches, CYP3A4 mRNA induction response must be observed in more than one donor to reduce the risk of false positives (Kenny et al., 2018); otherwise, at least one donor should exceed the defined threshold.

Performance of the established in vitro–in vitro correlation is affected by inclusion or exclusion of the potential effects of cytotoxicity, solubility, and non-specific binding at the concentrations tested. For example, Sun et al. (2017) reported <10% remaining of pleconaril after 24 h incubation at 4°C as well as 37°C likely due to the strong non-specific binding to incubation materials. In addition, a potential

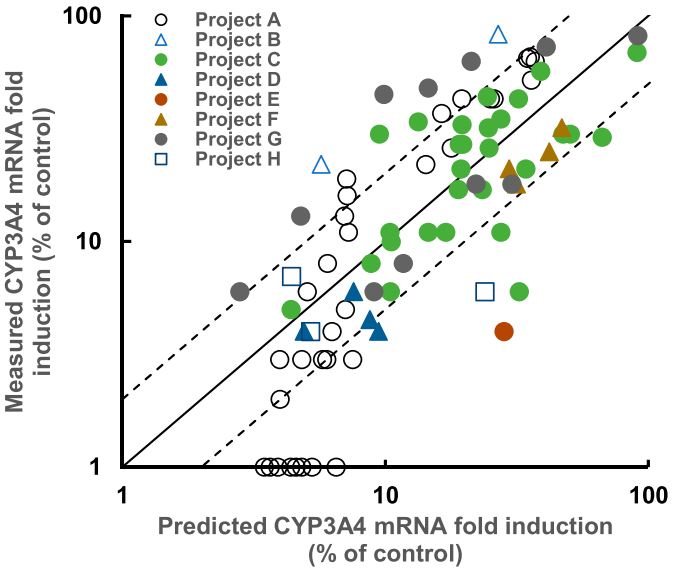

Fig. 2. Prospective prediction of CYP3A4 mRNA induction potential in human hepatocytes based on the PXR activation. CYP3A4 mRNA induction potential (% of control) in human hepatocytes (lot. 399) for 71 internal drug candidates at 0.1, 1, and/or 10 μM (mean, n = 3) predicted using the corresponding PXR activation (% of control) in DPX2 cells (mean, n = 3) were compared with the observed data (total data points = 90). Different symbols correspond to 8 early stage projects A–H. Solid and broken lines represent 1:1, and 1:2 or 2:1-correspondence, respectively.

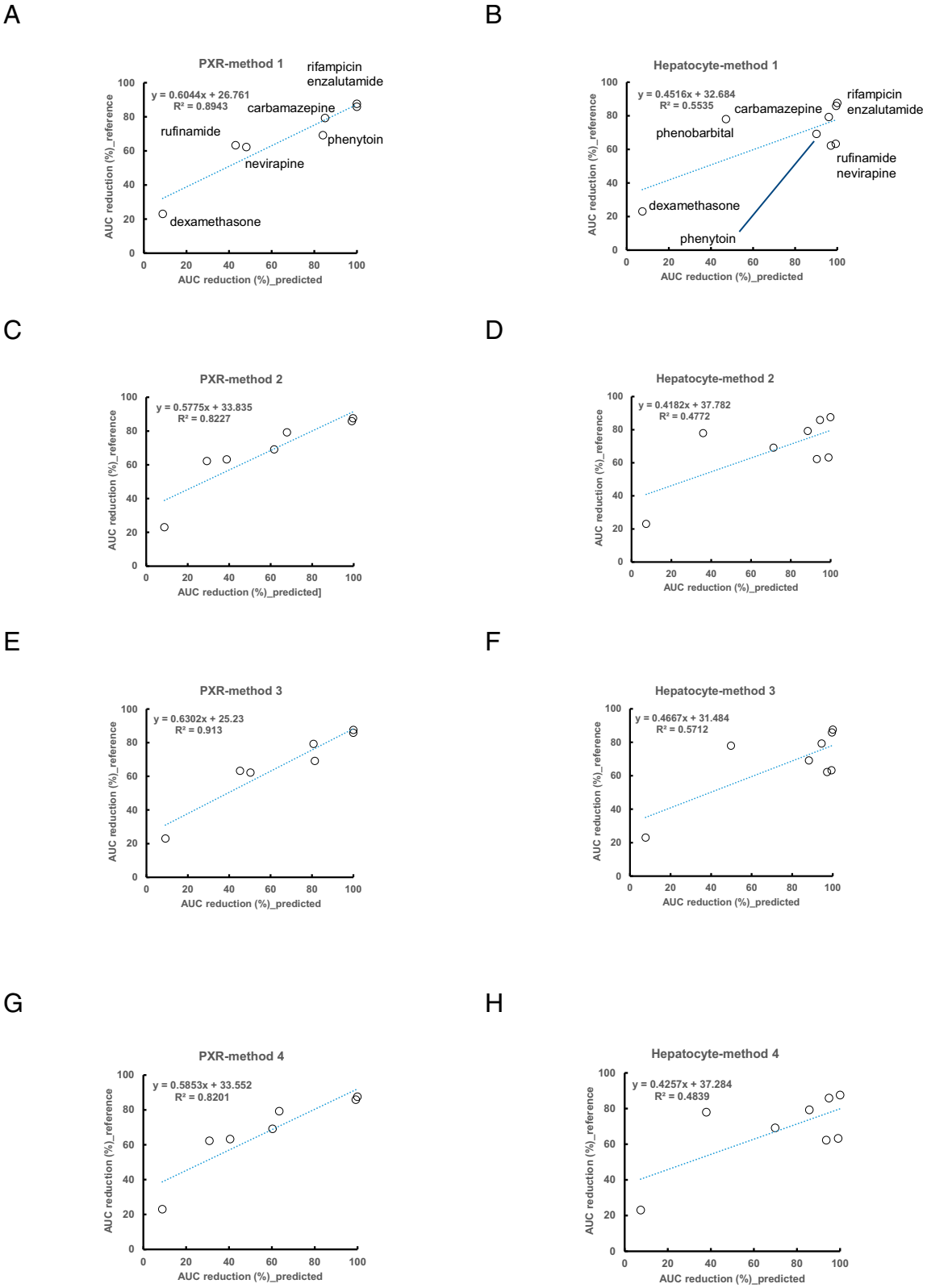

Fig. 3. Predicted versus observed AUC reduction (%) of the probe CYP3A4 substrate. The observed AUC reduction (%, mean) of the clinically used CYP3A4 substrates with the inducers (carbamazepine, dexamethasone, enzalutamide, nevirapine, phenobarbital, phenytoin, rifampicin, and rufinamide) (Table 2) were compared with the respective predictions (Table 3) based on the static induction model with the F2 method assuming interactions in the liver and the intestine (see Materials and Methods). Panels (A), (C), (E), and (G) show the in vitro–in vivo correlation based on PXR activation, while panels (B), (D), (F), and (H) show the correlation based on CYP3A4 mRNA induction. Methods 1, 2, 3, and 4 mean an employment of different [I]h values of Cave, Cave,u, Cmax, and Cmax,u for the static prediction, respectively, while the same calculation method was always employed for [I]g (Table 1). It should be noted that $N = 7$ for the PXR activation, while $N = 8$ for CYP3A4 induction since phenobarbital was tested only in the human hepatocytes. Measured CYP3A4 mRNA data using human hepatocyte batches 399 and/or HUM182641 in combination with historical data reported using three different liver donors (295, 312, 318) from Zhang et al. (2014) were applied for this correlation analysis.

TABLE 3

CYP3A4 induction DDI predictions based on the modified net effect model

(A) Input: PXR activation in DPX2 cells

	Ch					CYP3A4 substrates: AUC reduction (%)				
Drug name	Method 1 (Cave)	Method 2 (Cave,u)	Method 3 (Cmax)	Method 4 (Cmax,u)	Cg	Substrate	Method 1 (Cave)	Method 2 (Cave,u)	Method 3 (Cmax)	Method 4 (Cmax,u)
Carbamazepine	3.62	1.66	2.80	1.45	2.87	midazolam	85.0	67.8	80.7	63.4
Bosentan	2.36	1.03	5.32	1.09	9.02	simvastatin	93.7	85.5	97.2	86.3
Dexamethasone	1.00	1.00	1.01	1.00	1.30	panobinostat	8.83	8.76	9.16	8.85
Enzalutamide	49.9	2.47	57.8	2.70	93.3	midazolam	100.0	99.1	100.0	99.2
Nevirapine	1.82	1.33	1.90	1.36	2.17	itraconazole	48.1	29.2	50.3	30.8
Phenytoin	2.87	1.19	2.45	1.15	3.31	cyclosporine	84.0	61.6	81.4	60.3
Pleconaril	1.49	1.00	3.21	1.02	24.3	midazolam	94.5	92.0	97.4	92.1
Rifampicin	13.5	3.00	70.7	12.2	202	midazolam	99.9	99.7	100.0	99.9
Rufinamide	1.27	1.18	1.33	1.22	1.62	triazolam	43.0	38.8	45.2	40.5

(B) Input: CYP3A4 induction in human hepatocytes

	Ch					CYP3A4 substrates: AUC reduction (%)				
Drug name	Method 1 (Cave)	Method 2 (Cave,u)	Method 3 (Cmax)	Method 4 (Cmax,u)	Cg	Substrate	Method 1 (Cave)	Method 2 (Cave,u)	Method 3 (Cmax)	Method 4 (Cmax,u)
Carbamazepine	7.72	2.68	5.61	2.15	5.78	midazolam	95.9	88.5	94.4	85.7
Bosentan	63.3	2.25	200	4.98	370	simvastatin	100	99.8	100	99.9
Dexamethasone	1.00	1.00	1.01	1.00	1.25	panobinostat	7.36	7.31	7.64	7.39
Enzalutamide	14.5	1.40	16.6	1.47	26.4	midazolam	99.5	94.6	99.5	94.8
Nevirapine	15.0	6.62	16.4	7.17	21.0	itraconazole	96.9	93.0	97.2	93.6
Phenobarbital	1.80	1.39	1.93	1.45	1.61	verapamil	47.1	35.9	49.8	37.9
Phenytoin	3.71	1.27	3.11	1.21	4.35	cyclosporine	90.1	71.3	88.2	69.8
Pleconaril	1.11	1.00	1.50	1.01	6.32	midazolam	74.9	72.3	81.3	72.4
Rifampicin	21.2	4.23	114	19.0	326.9	midazolam	100	99.8	100	100
Rufinamide	10.0	6.97	11.8	8.15	21.6	triazolam	99.2	98.9	99.4	99.1

The AUC reduction of the CYP3A4 substrates in the presence of the inducers was predicted using a static induction model with F2 method. (A) and (B) were the corresponding predictions based on the PXR activation and the CYP3A4 mRNA induction, and methods 1, 2, 3, and 4 mean an employment of different [I]h values of Cave, Cave,u, Cmax, and Cmax,u for the static calculation, respectively. Cave was calculated as AUC/dosing interval during the treatment period of the inducers. The model input parameters were summarized in Supplemental Table 2. Note: Phenobarbital was tested only in the human hepatocyte induction study.

involvement of additional nuclear receptors in the CYP3A4 induction can alter the established correlation. For instance, a much higher CYP3A4 mRNA response (12-fold) compared with the PXR activation (2.04-fold) after incubation of mitotane at 10 μM (Supplemental Table 1) was observed. This supports the hypothesis of co-regulation of CYP3A4 induction by CAR as well as PXR as previously reported (Takeshita et al., 2013; in-house data). A CAR reporter gene assay could complement the use of the PXR assay and address underestimation of CYP3A4 mRNA induction potential based on only PXR transactivation, even though CAR activation is not necessarily caused by the ligand binding (Anderson et al., 2011).

CYP3A4 mRNA induction as % of the control response for 71 internal compounds at 0.1, 1, and/or 10 μM in drug discovery was predicted using the PXR activation data (Fig. 2). A limited number of false positive cases [19% of the data points (n = 90)] were observed. In particular, for the weak in vitro inducers showing <10% of the rifampicin control, PXR activation data can have value to complement hepatocyte induction profiles and for construction of quantitative structure-activity relationships. Nonetheless, improvement of the in vitro–in vitro correlation with 64% of cases within 2-fold error was demonstrated here compared with a previous report of only approximately 40% by Wei et al. (2016). Considering that we wished to assess the practical use of this approach in a screening mode in Drug Discovery where a short turnaround time is needed, the assay was intentionally evaluated using only one qualified hepatocyte batch (batch 399). We acknowledge that performing the assessment of CYP3A4 mRNA-inducing activity with additional batches of hepatocytes will be needed to provide further validity of the outcome.

Prediction of in vivo CYP3A4 induction based on in vitro PXR activation data has been previously reported (Fahmi et al., 2012), and data from human hepatocytes have been intensively studied using several static DDI calculation methods (Einolf et al., 2014). In this study, translatability was explored using a modified F2 method. This was done because of the difficulty in estimation of full induction parameters when cytotoxicity or solubility limitations are anticipated at higher concentrations (Kenny et al., 2018). Irrespective of the scenario used to estimate hepatic concentrations [I]h = Cave (method 1), Cave,u (method 2), Cmax (method 3), and Cmax,u

TABLE 4

Newly proposed thresholds for the assessment of CYP3A4 induction risk at preclinical phases

	% of control	Fold induction/activation
Assays	At least in one batch or on one assay occasion[a]	
CYP3A4 mRNA induction in human hepatocytes	≧(10%[b]or) 20%	≧2-fold
PXR activation in DPX2 cells	≧10%	—

[a] ≥2 donors for the hepatocyte induction study (Kenny et al., 2018).
[b] Some clinically relevant moderate/strong CYP3A4 inducers, such as carbamazepine and phenytoin, showed a weak induction potential in vitro. Stringent criteria would support a worst case scenario until clinical data are available.

(method 4), the in vivo CYP3A4 induction potential of the test drugs (carbamazepine, dexamethasone, enzalutamide, nevirapine, phenobarbital, phenytoin, rifampicin, and rufinamide) was reasonably estimated based on the in vitro data (Fig. 3; Table 1, Table 2, and Table 3). In our evaluation, the systemic exposure was employed instead of hepatic inlet concentration (which was deployed in the original net effect model) to avoid false positive induction predictions (Table 1). For the ten clinically used drugs tested in this study, the estimated unbound liver inlet concentrations were 1.97 (carbamazepine) to 29.5-fold (dexamethasone) higher than the respective unbound Cmax values (Supplemental Table 2). No significant difference in performance of the net effect model using Cave (methods 1/2) and Cmax (methods 3/4) was detected.

The insensitivity of in vitro–in vivo translatability to the effect of protein binding seen in this study can be attributed to the use of in vitro incubations without added protein. In addition, all test substances in this study have unbound fraction in human plasma (fu) within a technically measurable range of 0.01–0.66 (Supplemental Table 2). However, the overestimation of the in vivo CYP3A4 induction potential of pleconaril and bosentan may be linked to their low fu values of 0.01 and 0.02, respectively (Supplemental Table 2). These were exceptions to the good in vitro–in vivo correlation established in this study (Tables 2 and 3; Fig. 3; Supplemental Table 2 and Figure 2). For compounds with high protein binding, fu measurement could impact the predictability of induction as has been previously reported (Sun et al., 2017).

The moderate in vivo induction potential predicted using PXR activation for nevirapine and phenytoin was predicted in the strong induction category when based on the hepatocyte induction study results (Fig. 3; Table 2 and Table 3). Nevirapine potentially induces CYP2B6 by CAR activation, which cross-talks with the CYP3A4 induction cascade (Fan-Havard et al., 2013). Therefore, this may explain why the in vitro CYP3A4 induction potential could not be well-captured by DPX2 cells (Fig. 1; Supplemental Table 1).

Further causes of prediction errors may be poor estimation of inducer concentrations at the site where the induction DDI undergoes effects, such as auto-induction and time-dependent inhibition on CYP3A4 or other enzymes, and contributions of active uptake and biliary excretion to hepatic elimination. For example, reduction of systemic exposure of phenytoin at steady state compared with that after a single oral administration has been reported (Chetty et al., 1998), indicating auto-induction potential. Also, after co-medication of the CYP3A4 substrate simvastatin with oral administrations of bosentan, an AUC reduction was estimated to be 81% to 100%, which overestimated the clinical observation (40%) (Tables 2 and 3; Supplemental Figure 2). This may be attributed to the auto-induction of bosentan on CYP3A4/2C9 (Dingemanse and van Giersbergen, 2004) as well as an involvement of saturable hepatic active transport via organic anion transporting polypeptides 1B1 (Sato et al., 2018).

CYP2Cs, uridine 5′-diphospho-glucuronosyltransferases and transporters may also be induced by the PXR pathway; however, detecting these relatively weak signals using the reporter gene and human hepatocyte induction assays is challenging since induction of CYP3A4 in human hepatocytes is much more sensitive to PXR-mediated activation (Lu and Di, 2020). In this case, use of PBPK modeling to optimize the in vivo induction magnitudes to recover the historically reported induction DDI data at steady state would be a powerful tool for drug development. This method has already been postulated for P-glycoprotein (Yamazaki et al., 2019) and might be further used to validate additional in vitro induction readouts.

In conclusion, the successful use of PXR activation to estimate in vitro CYP3A4 induction potential with fewer false negative prediction cases was demonstrated using 13 clinically used drugs and 71 internal compounds. Moreover, even when characterization of full induction kinetics is limited by compound properties, such as cytotoxicity and solubility, reasonable translatability of the static induction risk assessment could be achieved with the F2 method and reasonable prediction performance based on the liver exit concentration was demonstrated, Nonetheless, certain limitations exist and pitfalls in early prediction need to be acknowledged, such as: 1) uncharacterized system biology on how CYP3A4 mRNA is regulated by PXR as well as other nuclear receptors including the negative feedback and 2) complex drug disposition affecting the unbound concentrations in the liver such as (auto-) induction of enzymes, active transport and binding. These results should enhance the assessment of induction risk and increase DDI prediction performance.

Acknowledgments

The authors wish to acknowledge Drs. Andres Olivares, Axel Pähler, Bianca van Groen, Caroline Rynn, Holger Fischer, Matthias Wittwer, Xiuli Li, and Yu Dai at F. Hoffmann-La Roche for their collaboration, the staffs at Pharmaron (Ningbo, China), and KaLy-Cell (Plobsheim, France) and Corning Life Sciences Discovery Labware (Woburn, MA), who have supported generation of the PXR activation and CYP mRNA induction data used in these analyses, respectively.

Authorship Contributions

Participated in research design: Ekiciler, Chen, Bo, Donzelli, Umehara.
Conducted experiments: Ekiciler, Chen, Bo.
Performed data analysis: Ekiciler, Chen, Bo, Umehara.
Wrote or contributed to the writing of the manuscript: Ekiciler, Chen, Bo, Pugliano, Donzelli, Parrott, Umehara.

References

Anderson LE, Dring AM, Hamel LD, and Stoner MA (2011) Modulation of constitutive androstane receptor (CAR) and pregnane X receptor (PXR) by 6-arylpyrrolo[2,1-d][1,5]benzothiazepine derivatives, ligands of peripheral benzodiazepine receptor (PBR). *Toxicol Lett* **202**: 148–154.

Bolleddula J, Ke A, Yang H, and Prakash C (2021) PBPK modeling to predict drug-drug interactions of ivosidenib as a perpetrator in cancer patients and qualification of the Simcyp platform for CYP3A4 induction. *CPT Pharmacometrics Syst Pharmacol* **10**:577–588.

Chetty M, Miller R, and Seymour MA (1998) Phenytoin auto-induction. *Ther Drug Monit* **20**:60–62.

Davies M, Peramuhendige P, King L, Golding M, Kotian A, Penney M, Shah S, and Manevski N (2020) Evaluation of In Vitro Models for Assessment of Human Intestinal Metabolism in Drug Discovery. *Drug Metab Dispos* **48**:1169–1182.

Dingemanse J and van Giersbergen PL (2004) Clinical pharmacology of bosentan, a dual endothelin receptor antagonist. *Clin Pharmacokinet* **43**:1089–1115.

Einolf HJ, Chen L, Fahmi OA, Gibson CR, Obach RS, Shebley M, Silva J, Sinz MW, Unadkat JD, Zhang L et al. (2014) Evaluation of various static and dynamic modeling methods to predict clinical CYP3A induction using in vitro CYP3A4 mRNA induction data. *Clin Pharmacol Ther* **95**:179–188.

Einolf HJ, Lin W, Won CS, Wang L, Gu H, Chun DY, He H, and Mangold JB (2017) Physiologically Based Pharmacokinetic Model Predictions of Panobinostat (LBH589) as a Victim and Perpetrator of Drug-Drug Interactions. *Drug Metab Dispos* **45**:1304–1316.

Fahmi OA, Hurst S, Plowchalk D, Cook J, Guo F, Youdim K, Dickins M, Phipps A, Darekar A, Hyland R et al. (2009) Comparison of different algorithms for predicting clinical drug-drug interactions, based on the use of CYP3A4 in vitro data: predictions of compounds as precipitants of interaction. *Drug Metab Dispos* **37**:1658–1666.

Fahmi OA, Raucy JL, Ponce E, Hassanali S, and Lasker JM (2012) Utility of DPX2 cells for predicting CYP3A induction-mediated drug-drug interactions and associated structure-activity relationships. *Drug Metab Dispos* **40**:2204–2211.

Fan-Havard P, Liu Z, Chou M, Ling Y, Barrail-Tran A, Haas DW, Taburet AM, and Group AS; ANRS12154 Study Group (2013) Pharmacokinetics of phase I nevirapine metabolites following a single dose and at steady state. *Antimicrob Agents Chemother* **57**:2154–2160.

Hariparsad N, Ramsden D, Taskar K, Badée J, Venkatakrishnan K, Reddy MB, Cabalu T, Mukherjee D, Rehmel J, Bolleddula J, , et al. (2022) Current Practices, Gap Analysis, and Proposed Workflows for PBPK Modeling of Cytochrome P450 Induction: An Industry Perspective. Clin Pharmacol Ther **112**:770–781.

Hakkola J, Hukkanen J, Turpeinen M, and Pelkonen O (2020) Inhibition and induction of CYP enzymes in humans: an update. *Arch Toxicol* **94**:3671–3722.

Huang SM, Abernethy DR, Wang Y, Zhao P, and Zineh I (2013) The utility of modeling and simulation in drug development and regulatory review. *J Pharm Sci* **102**:2912–2923.

Kanebratt KP and Andersson TB (2008) Evaluation of HepaRG cells as an in vitro model for human drug metabolism studies. *Drug Metab Dispos* **36**:1444–1452.

Kenny JR, Ramsden D, Buckley DB, Dallas S, Fung C, Mohutsky M, Einolf HJ, Chen L, Dekeyser JG, Fitzgerald M et al. (2018) Considerations from the Innovation and Quality Induction Working Group in Response to Drug-Drug Interaction Guidances from Regulatory Agencies: Focus on CYP3A4 mRNA In Vitro Response Thresholds, Variability, and Clinical Relevance. *Drug Metab Dispos* **46**:1285–1303.

Klammers F, Goetschi A, Ekiciler A, Walter I, Parrott N, Fowler S, and Umehara K (2022) Estimation of Fraction Metabolized by Cytochrome P450 Enzymes Using Long-Term Cocultured Human Hepatocytes. *Drug Metab Dispos* **50**:566–575.

Lehmann JM, McKee DD, Watson MA, Willson TM, Moore JT, and Kliewer SA (1998) The human orphan nuclear receptor PXR is activated by compounds that regulate CYP3A4 gene expression and cause drug interactions. *J Clin Invest* **102**:1016–1023.

Livak KJ and Schmittgen TD (2001) Analysis of relative gene expression data using real-time quantitative PCR and the 2(-Delta Delta C(T)) Method. *Methods* **25**:402–408.

Lu C and Di L (2020) In vitro and in vivo methods to assess pharmacokinetic drug- drug interactions in drug discovery and development. *Biopharm Drug Dispos* **41**:3–31.

Luo G, Cunningham M, Kim S, Burn T, Lin J, Sinz M, Hamilton G, Rizzo C, Jolley S, Gilbert D et al. (2002) CYP3A4 induction by drugs: correlation between a pregnane X receptor reporter gene assay and CYP3A4 expression in human hepatocytes. *Drug Metab Dispos* **30**:795–804.

Luzon E, Blake K, Cole S, Nordmark A, Versantvoort C, and Berglund EG (2017) Physiologically based pharmacokinetic modeling in regulatory decision-making at the European Medicines Agency. *Clin Pharmacol Ther* **102**:98–105.

Masica AL, Mayo G, and Wilkinson GR (2004) In vivo comparisons of constitutive cytochrome P450 3A activity assessed by alprazolam, triazolam, and midazolam. *Clin Pharmacol Ther* **76**:341–349.

Njuguna NM, Umehara KI, Huth F, Schiller H, Chibale K, and Camenisch G (2016) Improvement of the chemical inhibition phenotyping assay by cross-reactivity correction. *Drug Metab Pers Ther* **31**:221–228.

Sato M, Ochiai Y, Kijima S, Nagai N, Ando Y, Shikano M, and Nomura Y (2017) Quantitative Modeling and Simulation in PMDA: A Japanese Regulatory Perspective. *CPT Pharmacometrics Syst Pharmacol* **6**:413–415.

Sato M, Toshimoto K, Tomaru A, Yoshikado T, Tanaka Y, Hisaka A, Lee W, and Sugiyama Y (2018) Physiologically Based Pharmacokinetic Modeling of Bosentan Identifies the Saturable Hepatic Uptake As a Major Contributor to Its Nonlinear Pharmacokinetics. *Drug Metab Dispos* **46**:740–748.

Sun Y, Chothe PP, Sager JE, Tsao H, Moore A, Laitinen L, and Hariparsad N (2017) Quantitative Prediction of CYP3A4 Induction: Impact of Measured, Free, and Intracellular Perpetrator Concentrations from Human Hepatocyte Induction Studies on Drug-Drug Interaction Predictions. *Drug Metab Dispos* **45**:692–705.

Takeshita A, Igarashi-Migitaka J, Koibuchi N, and Takeuchi Y (2013) Mitotane induces CYP3A4 expression via activation of the steroid and xenobiotic receptor. *J Endocrinol* **216**:297–305.

Vieira ML, Kirby B, Ragueneau-Majlessi I, Galetin A, Chien JY, Einolf HJ, Fahmi OA, Fischer V, Fretland A, Grime K et al. (2014) Evaluation of various static in vitro-in vivo extrapolation models for risk assessment of the CYP3A inhibition potential of an investigational drug. *Clin Pharmacol Ther* **95**:189–198.

Yamashita F, Sasa Y, Yoshida S, Hisaka A, Asai Y, Kitano H, Hashida M, and Suzuki H (2013) Modeling of rifampicin-induced CYP3A4 activation dynamics for the prediction of clinical drug-drug interactions from in vitro data. *PLoS One* **8**:e70330.

Yamazaki S, Costales C, Lazzaro S, Eatemadpour S, Kimoto E, and Varma MV (2019) Physiologically-Based Pharmacokinetic Modeling Approach to Predict Rifampin-Mediated Intestinal P-Glycoprotein Induction. *CPT Pharmacometrics Syst Pharmacol* **8**:634–642.

Yang J, Jamei M, Yeo KR, Tucker GT, and Rostami-Hodjegan A (2007) Prediction of intestinal first-pass drug metabolism. *Curr Drug Metab* **8**:676–684.

Wei Y, Tang C, Sant V, Li S, Poloyac SM, and Xie W (2016) A Molecular Aspect in the Regulation of Drug Metabolism: Does PXR-Induced Enzyme Expression Always Lead to Functional Changes in Drug Metabolism? *Curr Pharmacol Rep* **2**:187–192.

Zhang JG, Ho T, Callendrello AL, Clark RJ, Santone EA, Kinsman S, Xiao D, Fox LG, Einolf HJ, and Stresser DM (2014) Evaluation of calibration curve-based approaches to predict clinical inducers and noninducers of CYP3A4 with plated human hepatocytes. *Drug Metab Dispos* **42**:1379–1391.

Zhu Z, Kim S, Chen T, Lin JH, Bell A, Bryson J, Dubaquie Y, Yan N, Yanchunas J, Xie D et al. (2004) Correlation of high-throughput pregnane X receptor (PXR) transactivation and binding assays. *J Biomol Screen* **9**:533–540.

Address correspondence to: Dr. Kenichi Umehara, Roche Pharmaceutical Research and Early Development, Grenzacherstrasse 124, CH-4070 Basel, Switzerland. E-mail: kenichi.umehara@roche.com